Int J Adv Manuf Technol (2017) 91:1935–1944
DOI 10.1007/s00170-016-9933-1

ORIGINAL ARTICLE

Finite element and experimental analysis of machinability during machining of high-volume fraction SiCp/Al composites

L. Zhou[1,2] · **C. Cui**[1] · **P.F. Zhang**[1] · **Z.Y. Ma**[2]

Received: 6 June 2016 / Accepted: 18 December 2016 / Published online: 28 December 2016

Abstract The machinability, including machined surface, edge quality, and the distribution of the subsurface residual stress, was studied during the orthogonal cutting of high-volume fraction SiCp/Al composites by both finite element analysis and experiments. The effect of cutting parameters on surface roughness, sizes of edge breakout, and residual stress were investigated. The elastic-plastic constitutive model and Johnson–Cook damage model for the Al alloy matrix, and the elastic-brittle failure for SiC particle were implemented in the mechanical properties of composites during the cutting simulation. The results indicate that the surface morphology is primarily dependent on the fracture models of SiC particles, and the formation of the negative shear plain is the main reason of edge breakout. Due to the inhomogeneity in the composites, the distribution of surface and subsurface residual stress is not uniform, and the high residual stress was distributed in the interface between irregular particles and matrix. The average value of residual stress of SiC particle is similar to that of the matrix. The predicted machined surface morphology and edge breakout sizes correlated well with the experimental observation. This study highlights the important role of the fracture model of SiC particles on surface finish and the edge quality. It provides useful information for better understanding of the mechanics in machining of the SiCp/Al composites.

✉ Z.Y. Ma
zyma@imr.ac.cn

[1] School of Mechanical Engineering, Shenyang Ligong University, Shenyang 110159, China

[2] Institute of Metal Research, Chinese Academy of Sciences, Shenyang 110016, China

Keywords Composites · Orthogonal cutting · Finite element simulation · Machinability

1 Introduction

SiCp/Al composite possesses excellent combination of physical and mechanical properties, such as low density, high specific stiffness and strength, superior wear, and creep properties, and therefore is increasingly used in defense and aerospace structures [1–3]. The traditional machining methods of SiCp/Al composite are still very important in machining mechanical parts, although many new and improved production techniques, such as precision casting and net shape forming, have been used extensively [4]. Unfortunately, the heterogeneity and the abrasive nature of SiC particle reinforcement make the machinability of these materials more difficult compared to the conventional metals and their alloys. Thus, the wider applications of SiCp/Al composites have often been hindered due to the difficulty and high cost associated with machining them into damage free composite parts with requisite tolerances and surface finish.

Machinability of work materials depends on their thermo-mechanical properties, structure, and compatibility with tool materials [5]. In the past decades, experimental machining of SiCp/Al composites has been extensively carried out, and most of them concentrated on the cutting force [6, 7], surface roughness [8, 9], subsurface damage [10], the tool adaptability [11–13], etc. Besides, numerical modeling has been used as a tool to understand the mechanics associated with machining processes. An experimental physical model on the cutting characteristics of metal matrix composites was presented by Davim et al. [14], and the chip compression ratio, chip deformation, friction angle, shear angle, normal stress, and shear stress were evaluated by using Merchant equation. A number

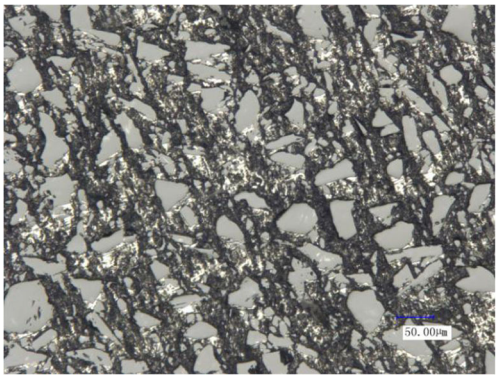

Fig. 1 Microstructure of SiCp/Al composite

of attempts have been made in modeling machining processes of composites. Chinmaya et al. [15] developed a multistep 3-D finite element model to investigate the cutting force and subsurface damage for machining of A359/SiC/20p composite. However, in their work, the effect of particle morphology on the machining properties of composite was not considered, since the finite element model was established based on spherical particle assumption. Furthermore, the two-dimensional orthogonal cutting process was simulated using the finite element method, and the tool–particle interaction was studied by considering particles along, above and below the cutting path by Zhu and Kishawy [16] and Pramanik et al. [17].

Surface integrity is one of the important factors for evaluating workpiece quality as it influences the functional characteristics of workpiece such as fatigue strength, corrosion resistance, wear resistance, and compatibility [18]. Since the mechanical properties of SiC particles are completely different from those of the Al alloy matrix, the machining mechanics and damage mechanism of SiCp/Al composites are very complicated. According to the literature, the SiCp/Al composites subjected to machining investigations usually had SiC volume fraction of 20 vol%, and there is very little literature regarding the machining of higher volume fraction SiCp/Al composites. Moreover, the cutting mechanism for SiCp/Al composites is not fully understood.

In this study, a micromechanical model is presented to characterize the relationship between the macroscopic behaviors and microstructure deformation and fracture properties by investigating the surface and subsurface damage mechanics, edge breakout, and residual stress. Additionally, the numerical results were compared to the orthogonal cutting experiments at different cutting depths and speeds to investigate the effects of various cutting parameters on the surface roughness, residual stress, and edge breakout size.

2 Experimental details

The orthogonal cutting experiments were conducted on 55 vol% SiCp/6061Al composite, produced by powder metallurgy technique, and the average particle sizes of 60 and 20 μm were used as the reinforcements. A typical microstructure of this material is shown in Fig. 1. From the figure, it can be observed that both the large SiC particles and small SiC particles are homogeneously distributed in aluminum matrix. The experimental samples with dimension of $60 \times 50 \times 5$ mm^3 were prepared by cutting in a wire electrical discharge machine. The orthogonal cutting tests were carried on a high-precision vertical machining center EUMA ME650 with polycrystal diamond (PCD) tool in dry conditions. The cutting speed and depth were taken into consideration for factors influencing surface integrity, corresponding to cutting speed of 4, 8, 12, 16, and 20 m min^{-1}, and cutting depth of 0.03, 0.06, 0.09, 0.12, and 0.15 mm. The total cutting distance and cutting width were 60 and 5 mm, respectively. In order to investigate the detailed surface morphology, fracture morphology, and the size of edge breakout, scanning electron microscopy (SEM) and a digital optical microscope (KEYENCE, VHX-1000) were used to examine the surface of the samples.

3 Finite element modeling procedure

3.1 Finite element model

By imitating the real particle morphology from the typical micrographs of SiCp/Al composites (see Fig.1), a microstructure-based two-dimensional plane strain and random particles model was built with the aid of Abaqus/Explicit, as shown in Fig. 2. It can be seen that the morphology of SiC particles was polygonal, and the particle size and

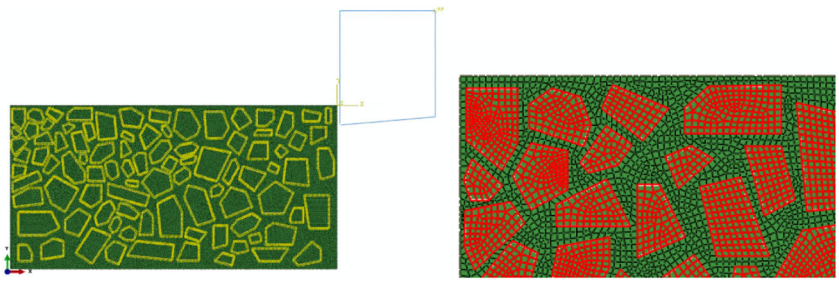

Fig. 2 **a** Finite element model of orthogonal cutting of SiCp/Al composite and **b** local zooming of **a**

Table 1 Material constants for Johnson–Cook constitutive model of 6061Al alloy

A (MPa)	*B* (MPa)	*C*	*n*	*m*
240	200	0.005	0.2	2

From [19]

Table 2 Mechanical properties applied in finite element computation

Materials properties	Al alloy matrix	SiC particles
E, Young's modulus (GPa)	70.6	420
ν, Poisson's ratio	0.34	0.14
Coefficient of thermal expansion (K^{-1})	23.6×10^{-6}	4.9×10^{-6}
ρ, Density (kg m^{-1})	2.7×10^{3}	3.13×10^{3}
k, Thermal conductivity (W m^{-1} K^{-1})	180	81
C_P, specific heat (J kg^{-1} K^{-1})	880	427

From [20]

Table 3 Johnson–Cook damage parameters of Al alloy matrix

d_1	d_2	d_3	d_4	d_5
−0.77	1.45	−0.47	0.0	1.60

From [21]

volume fraction are constant with the experimental data. Then, the established model can be applied to analyze the effect of reinforced SiC particles on the machinability of SiCp/6061Al composites. In this model, the matrix and the particles are modeled separately and the 4-node plane strain bilinear quadrilateral elements (CPE4RT) in ABAQUS were adopted to mesh both the matrix and SiC particles. The surface of particles ties with the surface of matrix, and the particles and matrix were bonded together by this way. In order to show the mesh clearly, the upper left corner in Fig. 2a has been amplified as shown in Fig. 2b.

In this work, the workpiece was constrained in any direction on the bottom surface, and the tool moved at a specified cutting speed and cutting depth, which was controlled by a reference point and the machining forces were measured as reaction forces.

3.2 Material constitutive equation

Traditionally, particle reinforced metal matrix composites is modeled as homogeneous medium in classic continuum medium, and such a modeling method does not take into account the deformation and failure mechanisms during machining of SiCp/Al composites. It is well-known that the mechanical properties, deformation, and fracture models of SiC particles are completely different from those of the Al alloy matrix. In this work, during the machining process, the Johnson–Cook constitutive equation was implemented to model the flow behavior of Al alloy. Here, the Johnson–Cook model can be expressed as:

$$\sigma = [A + B\varepsilon^n]\left[1 + C\ln\left(\frac{\dot{\varepsilon}}{\dot{\varepsilon}_0}\right)\right]\left[1 - \left(\frac{T - T_r}{T_m - T_r}\right)^m\right] \quad (1)$$

where σ is the flow stress, ε is the plastic strain, $\dot{\varepsilon}$ is the strain rate, $\dot{\varepsilon}_0$ is the reference plastic strain rate, A is the yield stress at reference temperature and strain rate, B is the strain hardening coefficient, n is the strain hardening exponent, C is the strain rate sensitivity coefficient, and m is the thermal softening exponent. T is the workpiece temperature, and T_m and T_r are the material melting and room temperature, respectively.

The material constants of 6061Al alloy matrix are obtained from the split Hopkinson pressure bar (SHPB) test over wide temperatures and strain rates by Fan et al. [19], and listed in Table 1. Additionally, the SiC particles are modeled as an isotropic perfectly elastic material following the generalized Hook's Law, and brittle cracking model was used. The cutting tool was treated as a perfectly rigid body for its high elastic modulus. The material parameters applied in the finite element computational analysis are listed in Table 2 [20].

3.3 Fracture model

Johnson–Cook damage criterion, available in Abaqus/Explicit, was utilized to describe the chip separation behavior for all the Al alloy matrix elements. Johnson–Cook criterion

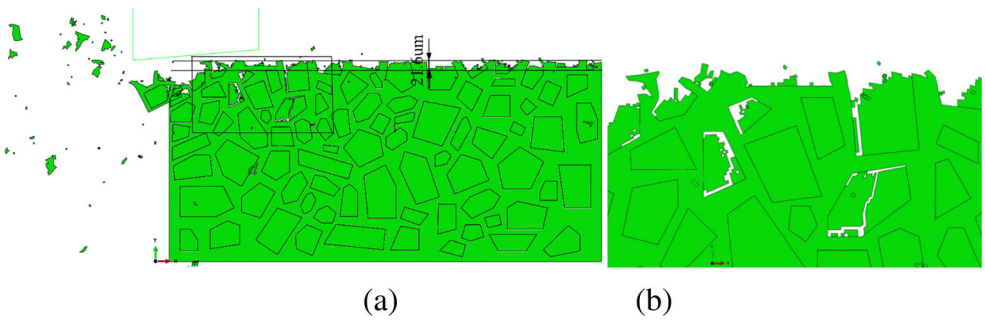

Fig. 3 **a** Surface morphology and **b** local zooming of **a**

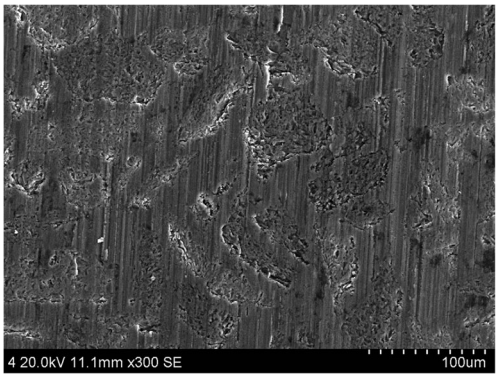

Fig. 4 Typical machined surface morphology of SiCp/6061Al composites

for damage initiation is met when the following condition is satisfied [21]:

$$w_D = \sum \frac{\Delta \varepsilon^p}{\varepsilon^f} = 1 \tag{2}$$

where

$$\varepsilon^f = [d_1 + d_2 \exp(-d_3 \eta)]\left[1 + d_4 \ln\left(\frac{\varepsilon^p}{\varepsilon_0}\right)\right]\left[1 + d_5\left(\frac{T - T_{\text{transition}}}{T_{\text{melt}} - T_{\text{transition}}}\right)\right] \tag{3}$$

Here, $\Delta\varepsilon^p$ is the change in the equivalent plastic strain during each integration cycle and ε^f is the fracture strain, $d_1 - d_5$ are the failure parameters, $\eta = -p/q$is the stress triaxiality, p is the pressure stress, q is the von Mises equivalent stress, ε^p and ε_0 are the plastic strain rate and reference strain rate, respectively, $T$and T_{melt} are the current temperature and melting temperature, and $T_{transition}$ is the transition temperature defined as the one at or below which there is no

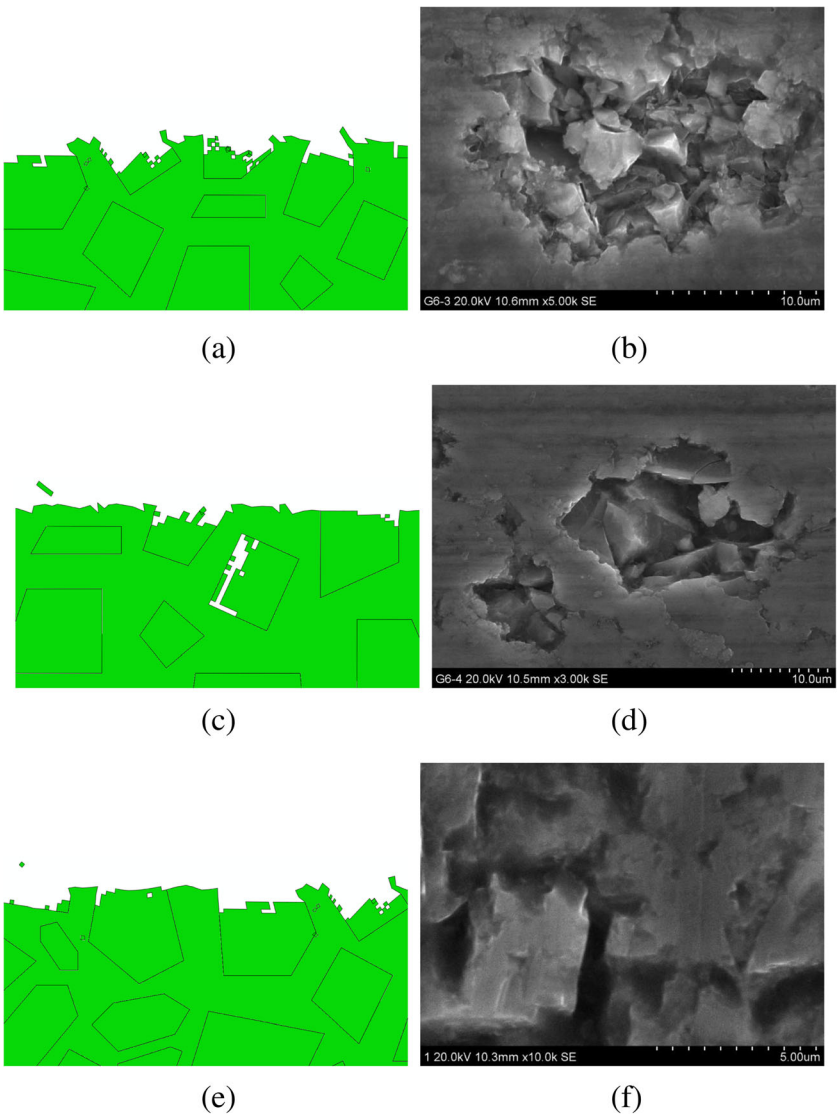

Fig. 5 Various removal models of SiC particles by simulation and experiment: **a**, **b** crushing, **c**, **d** part crushing, **e**, **f** cutting through, **g**, **h** fracture, and **i**, **j** pulling out

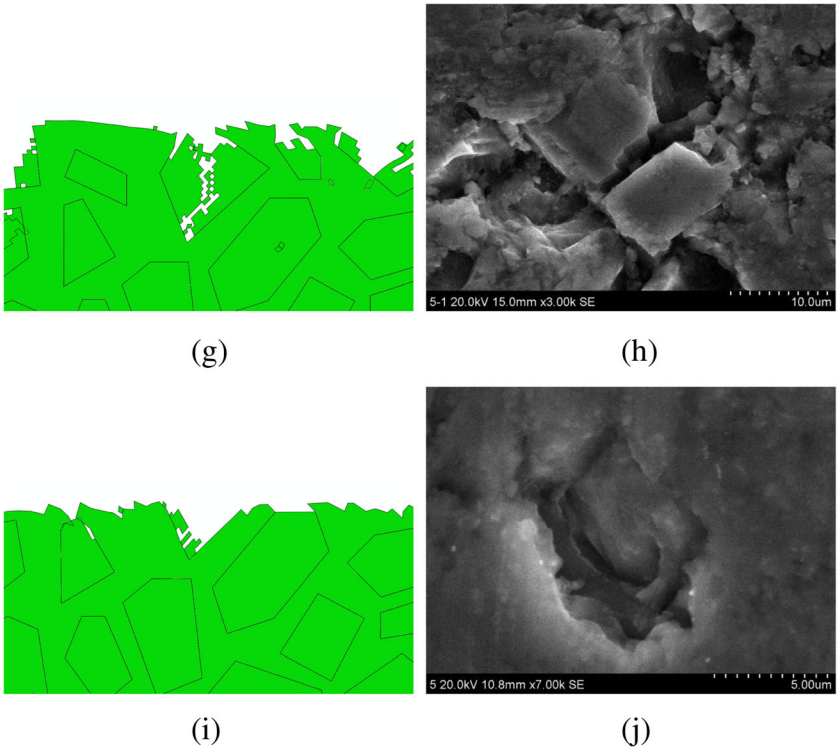

Fig. 5 (continued)

temperature dependence on the expression of the fracture strain ε^f. The failure parameters $d_1 - d_5$ adopted in the simulation are listed in Table 3.

4 Results and discussion

4.1 Surface topography

The surface topography of the cut specimens was examined to reveal the fracture behavior of the high-volume fraction SiCp/6061Al composites induced by orthogonal cutting. Figure 3 shows the typical topography of machined surface and fragmented chips by the FE model. From the figure, it can be seen that the machined surface is very irregular and the formation of machined surface includes the ductile remove of matrix and brittle fracture of the particles. At the same time, the edge fracture and subsurface damage were clearly visible. Due to the high localized stress generated during machining, the presence of plastic deformation at the surface is inevitable, and the damage introduced into the workpiece extends below the machined surface. It is clear that the different failure mechanisms of particles

Table 4 Values of the surface roughness and edge defects sizes as a function of the cutting parameters

Cutting speed (m min^{-1})	Cutting depth (mm)	Surface roughness (μm)		Edge defects size (μm)			
		Experimental	Calculated	Width		Height	
				Experimental	Calculated	Experimental	Calculated
4		26.5	21.3	123.1	114.2	78.5	71.6
8		29.2	22.1	132.5	121.3	87.4	68.4
12	0.09	26.8	21.7	129.3	118.5	90.5	74.1
16		25.9	20.6	145.5	126.2	89.2	75.2
20		28.3	21.5	150.4	121.4	88.9	76.9
	0.03	26.5	22.1	123.8	114.1	78.1	71.4
	0.06	29.4	27.6	146.7	125.8	84.2	74.1
12	0.09	38.8	30.3	152.1	134.4	89.3	79.3
	0.12	45.9	40.2	168.2	144.9	97.7	89.6
	0.15	62.3	47.4	184.4	165.2	102.1	90.5

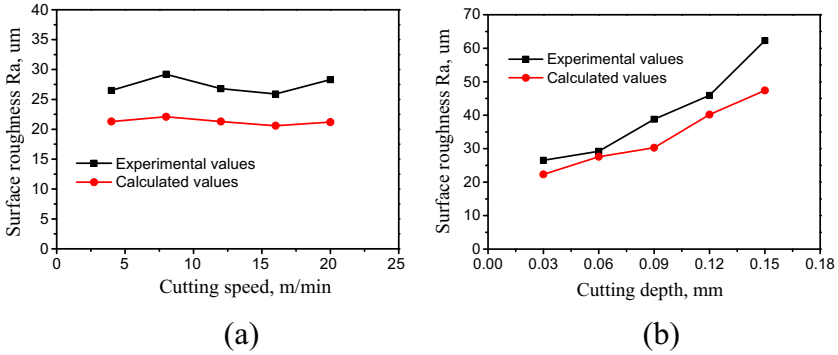

Fig. 6 Effect of cutting parameters on surface roughness, **a** speed and **b** depth

and matrix play an important role during the machining of composites.

To obtain clearer view of the subsurface damage, the upper left corner in Fig. 3a is zoomed in Fig. 3b. The figure shows that fracture and crush take place in the particles, and voids and cracks initiate around the particles due to plastic deformation in the matrix material. The subsurface damage is about 100 μm below the machined surface, which is almost the same reported previously by Gallab et al. [10]. A typical view of the machined SiCp/6061Al composites surface topography is shown through SEM images (Fig. 4). It is evident that the surface defects appeared around the SiC particles, while the ductile remove occurred in the matrix, which is consistent with the experimental results.

Different removal models of SiC particles obtained from numerical modeling are compared to orthogonal cutting experimental results, as shown in Fig. 5a–j. Analyzing the local removal models, we found that the SiC particles are either crushing (see Fig. 5a, b), part crushing (see Fig. 5c, d), cutting through (see Fig. 5e, f), fracture (see Fig. 5g, h), or pulling out (see Fig. 5i, j).

After machining, the machined surface roughness by FE calculated is shown in Fig. 3a, and the values of the surface roughness obtained for experimental and calculation are listed in Table.4. Figure 6a, b shows the variations of measured surface finish (Ra) from experiment and calculation with cutting speed and depth. As expected, the influence of cutting speed on surface roughness was not obvious, and the surface roughness increased with the increase of cutting depth for both experimental and calculated results. This agrees with the experimental results by Wang et al. [22], where the volume fraction of SiC particles in composites was 65%, and the influence of milling speed on surface roughness was also not obvious.

In general, the surface roughness slightly decreases with the increase in cutting speed due to lower flow stress of Al alloy matrix at higher cutting speed. In this study, the volume fraction of SiC particles in the composite is very high, and the thermal softening of aluminum matrix is not obvious with increasing cutting speed. While increasing of the cutting depth, the higher cutting force will induce the cutting action tends to be more unstable during machining and results in greater surface roughness values.

In addition, it is worth noting that there are some similar phenomena in Fig. 6a, b, and the simulated values are smaller than the experimental values. These can be explained by the present simulation model. In this model, the material is assumed to have no defects and the interface between the Al matrix and the SiC particles has not been considered. In fact, besides many microscopic material defects such as cracks or pores, the tool wear has a strong influence on cutting force and

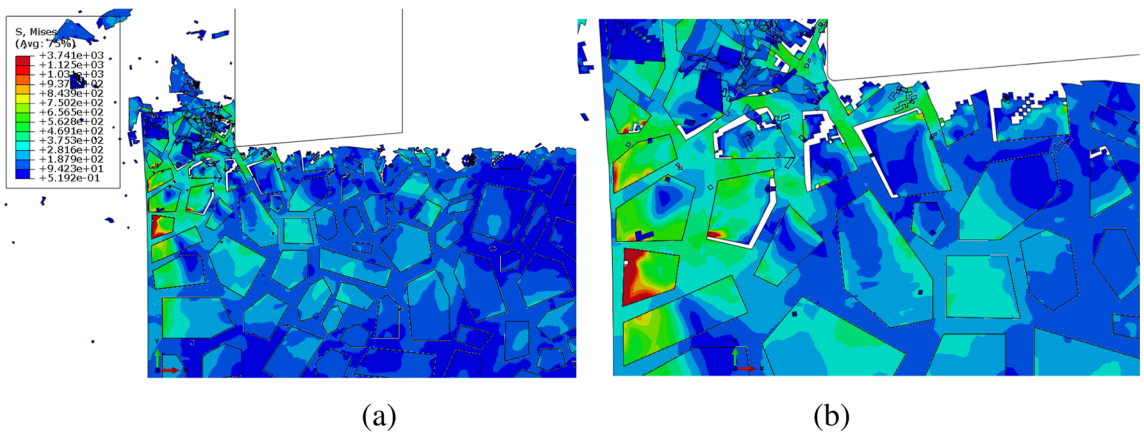

Fig. 7 **a** Crack initiates and propagates when the tool approaches the end of the workpiece and **b** local zooming of **a**

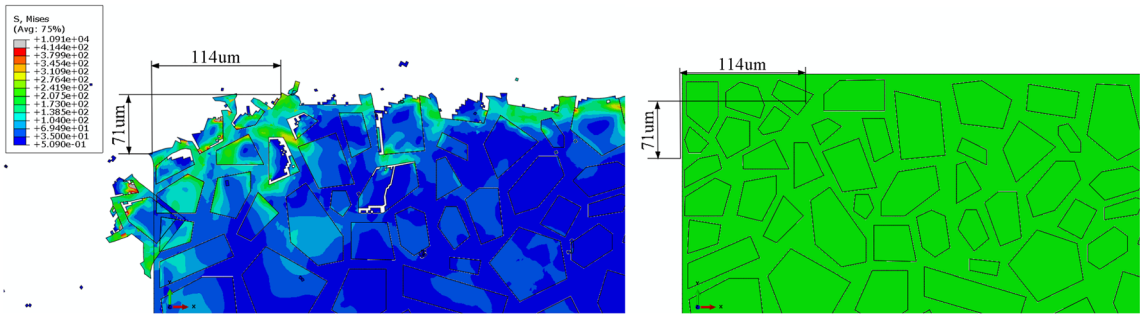

Fig. 8 **a** Edge fracture of SiCp/Al composites by FE simulation and **b** original microstructure

surface roughness obtained from the experiments than that in the calculation.

4.2 Edge topography

When the tool approaches the end of the workpiece, the negative shear plain is formed and the crack initiates and propagates along the interface between the particles and matrix; in the case of large particles, the crack will also occur in the particles, as shown in Fig. 7. Figure 7b is the local amplified figure of Fig. 7a. The distribution of stress reveals that during the cutting process, the maximum cutting force is distributed in the sharp corner of the SiC particles; after the crack initiate, the stress relaxed.

Figure 8a shows that eventually the tool cuts through the workpiece and the irregular edge morphology is formed. Compared to the original microstructure in Fig. 8b, it can be observed that the fracture of particles, interface debonding, and the failure of matrix take place. Figure 9 gives the rough edge morphology and SEM fractographs after machining of SiCp/Al composite. Different from the ductile material, there is an edge breakout with the width being larger than the height for the composite (see Fig. 9a), and the height and width of the edge defects are listed in Table 4. Figure 9b shows the fractographs of the edge, and it can be seen that the brittle fracture of the SiC particles occurred and some facets were found in the larger SiC particle. In addition, debonded interface and ductile failure of the Al matrix could be also observed.

The influences of cutting speed and depth on the height and width of edge breakout for simulation and experiment are depicted in Fig. 10. It is observed that the height and width of edge breakout increase when the cutting depth is increased. However, the cutting speed has a very small effect on the sizes of edge breakout. Similar trend has also been observed with all the experimental machining parameters. In addition, from Fig. 10a, b, it is clear that the simulated values for both the width and height are smaller than the experimental values. Our previous experimental results revealed that the cutting force increases with the depth of cut due to the increase of material removal rate. On the contrary, the cutting speed has no significant effect on the cutting force, which is attributed to the little thermal softening effect of Al matrix during machining of the high-volume fraction SiCp/Al composites. The edge breakout formation depends significantly on the cutting force, and the change tendency of edge breakout sizes with cutting parameters is quite similar to that of the cutting force [23]. Therefore, in order to obtain a fine surface and edge quality and precise machining accuracy, a smaller cutting depth must be used in machining of SiCp/Al composites; on the contrary, the cutting speed can be adopted as high as possible.

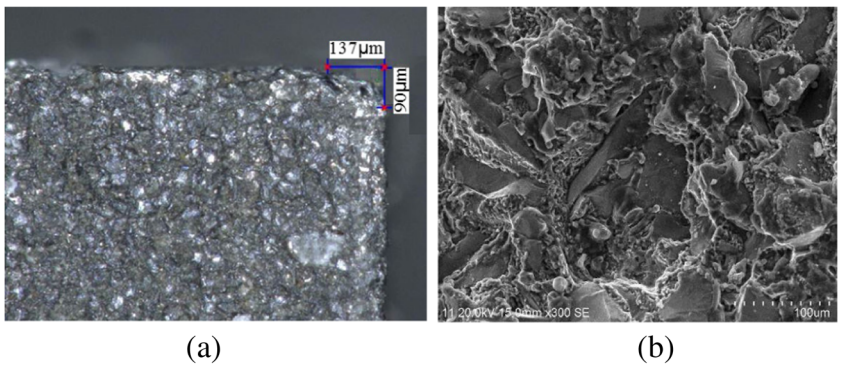

Fig. 9 **a** Edge fracture of SiCp/Al composites after machining and **b** SEM fractograph

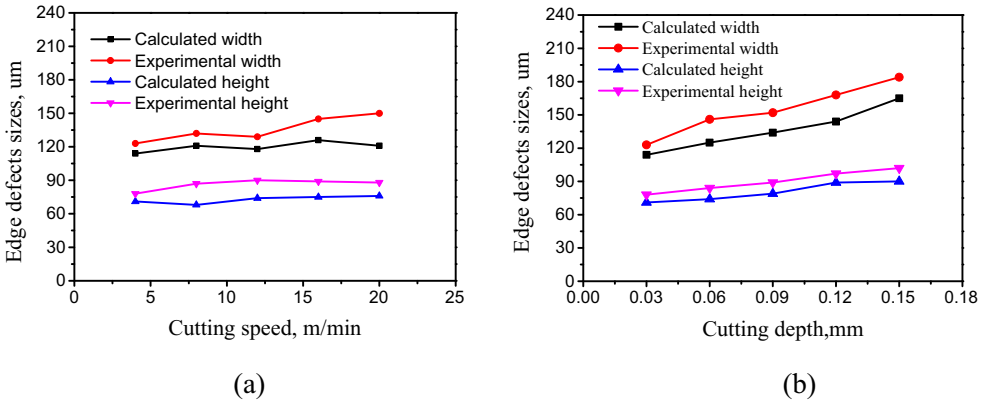

Fig. 10 Influence of **a** cutting speed and **b** cutting depth on edge breakout sizes

4.3 Residual stress

A total of two step analysis was performed to study the effects of cutting depth and speed on induced residual stresses. In the first step, the tool plows the workpiece surface which is accomplished in ABAQUS/Explicit, and the transient stress and strain of the workpiece were computed in a dynamic analysis processing. In the step 2, transient stresses were relaxed by conversion constraint conditions, and then the residual stress can be computed.

Figure 11 shows the calculated residual stresses after machining. It can be seen that the residual stress decreases with the increase of the distance from the machined surface and is induced up to 100 μm below the machined surface. In the same time, due to the complex microstructure of the composite, the distribution of residual stress is uneven, and the local stress concentrations appear at the interfaces between the matrix and the particles, especially in the areas where two particles are close to each other. In addition, in this model, the volume fraction of the particles is very similar to that of matrix, and the value of residual stress in the particles is also similar to that in the matrix, which can be explained by the stress equilibrium condition of the microscopic [24]:

$$(1-V)\sigma^M + V\sigma^P = 0 \tag{4}$$

where V is the volume content of the reinforcement, σ^M and σ^P are the residual stresses of matrix and particle, respectively.

To obtain the distribution of the residual stress along the depth direction, the residual stress profiles at three locations of the machined surface (1, 2, and 3) were collected and the average values were calculated, as described in Fig. 11. Moreover, to obtain the residual stress at different depths, the residual stress of 10 points at each position was extracted in the depth direction as shown in Fig. 11.

Figure 12 shows the effect of cutting parameters on residual stress profiles at machined surface layer. It can be seen that the more compressive residual stress occurs at the surface and about 30 μm below the machined surface, which agrees with the earlier results by Dabade et al. and Pramanik et al. [25, 26], and the magnitude of the residual stress is close to the measured results obtained in [26]. Moreover, with the increase of the distance from the machined surface, the compressive residual stress turns to tensile residual stress. The calculated residual stress profiles are hook-shaped, and the similar trends in machining induced residual stress profiles were observed in machining of alloy materials [27, 28].

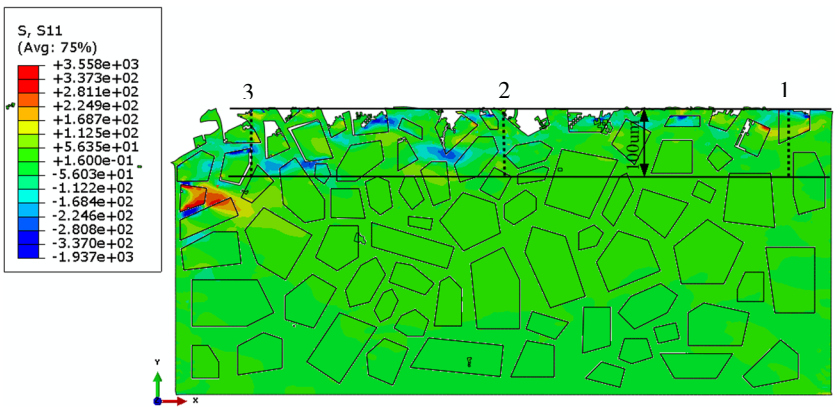

Fig. 11 Residual stress distribution after machining

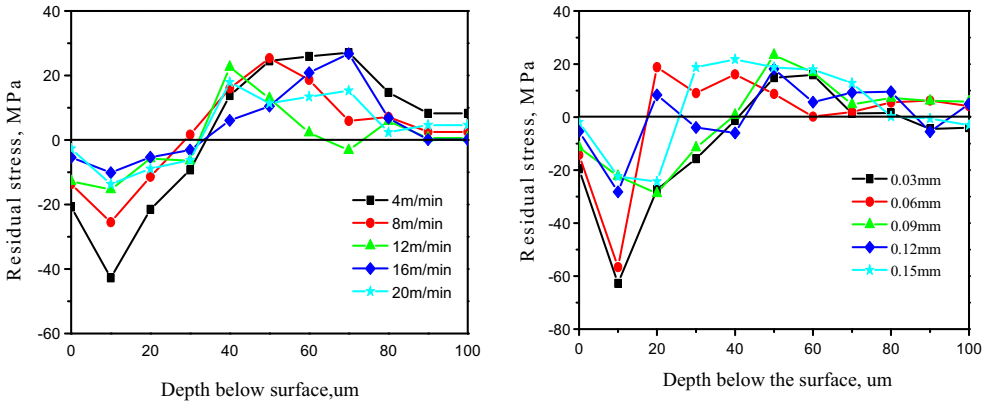

Fig. 12 Influence of cutting parameters on residual stress, **a** cutting depth and **b** cutting speed

In general, for monolithic metal or alloy materials, the residual stress profiles are beginning with a high tensile stress at the surface due to thermal strain. Capello [29] divided the mechanisms of residual stress generation into three categories: mechanical (plastic deformation), thermal (thermal plastic flow), and physical (specific volume variation). Tensile residual stresses are caused by thermal effects and compressive stresses by mechanical effects related to the machining operation. The relatively small compressive stress measured on the surface of SiCp/Al composite indicates marginally higher influence of mechanical factors compared to thermal factors. These factors are the restriction of matrix flow due to presence of particles and high compression of matrix in between particles and tool [26].

On the other hand, in this study, the cutting speed is very low, and the cutting temperature is also low and thermal residual stress is much smaller than plastic residual stress, thus, a lower compressive residual stress occurs at the machined surface. Although the compressive stresses are introduced into the machined surfaces, a number of defects such as fracture and pull-out of particles were still present on the machined surface, and a damage-free surface is very difficult to achieve during machining of SiCp/Al composites. Meanwhile, from Fig. 12a, b, it can be observed that the effects of cutting speed and depth on residual stress are not significant, due to the complex microstructural effects. The internal stress and deformation mechanisms of SiCp/Al composites are more complicated and different from those of a monolithic material, and the mechanisms of residual stress generation are likely to be more complex for the composites. As a result, the effect of machining parameters on surface residual stress may not be the similar when the reinforced particles are present.

5 Conclusions

A micro-finite element model and orthogonal cutting experiment were carried out to study the machined surface, edge quality, and the distribution of the residual stress. The elastic–plastic constitutive model and Johnson–Cook damage model for the Al alloy matrix and the elastic-brittle failure for the SiC particle were implemented in the mechanical properties of composites during the cutting simulation. Good agreement was found between the experimental and calculated results. The following conclusions can be drawn:

1. The formation of machined surface consists of the ductile remove of matrix and brittle fracture of the particle, and the surface morphology is primarily dependent on the fracture models of SiC particles. The fracture model of particles includes crushing, part crushing, cutting through, fracture, and pulling out of SiC particles. The surface roughness increases with the increase of cutting depth, and the influence of cutting speed on surface roughness is not obvious for both experimental and calculated results.
2. Due to the brittle failure of SiC particles, the edge breakout takes place near the final exit position of the workpiece. The edge breakout size almost linearly increases with increasing cutting depth, while cutting speed has little effect on the sizes of edge breakout. Therefore, in precision cutting of SiCp/Al composites, cutting speed should be as high as possible, but not for the cutting depth.
3. After unloading, a lower compressive stress occurs at the machined surface of SiCp/Al composite, and the state of residual stress changes from compressive to tensile with the increasing of the distance from the machined surface. The effects of cutting speed and depth on residual stress is not significant; this is due to the complexity of the reinforcement mechanisms of SiC particles.

Acknowledgements The authors gratefully acknowledge the financial support by the National Natural Science Foundation of China (51175353) and the Key Subject Open Fund of Shenyang Ligong University (4771004kfx21).

References

1. Liu J, Li J, Xu CY (2014) Interaction of the cutting tools and the ceramic-reinforced metal matrix composites during micro-machining: a review. CIRP J Manuf Sci Technol 7:55–70
2. Umanath K, Palanikumar K, Selvamani ST (2013) Analysis of dry sliding wear behaviour of Al6061/SiC/Al2O3 hybrid metal matrix composites. Compos Part B: Eng 53:159–168
3. Dandekar CR, Shin YC (2012) Modeling of machining of composite materials: a review. Int J Mach Tools Manuf 57:102–121
4. Davim JP (2011) Machining of metal matrix composites. Springer press, London
5. Warner AEM, Bell JAE, Stephenson TF (1998) Opportunities for new graphitic aluminium metal matrix composite. Mater Sci Technol 14:843–850
6. Kannan S, Kishawy HA, Deiab I (2009) Cutting forces and TEM analysis of the generated surface during machining metal matrix composites. J Mater Process Technol 209:2260–2269
7. Davim JP, Baptista AM (2000) Relationship between cutting force and PCD cutting tool wear in machining silicon carbide reinforced aluminium. J Mater Process Technol 103:417–423
8. Ge YF, Xu JH, Yang H, Luo SB, Fu YC (2008) Workpiece surface quality when ultra-precision turning of SiCp/Al composites. J Mater Process Techol 203:166–175
9. Palanikumar K, Karthikeyan R (2007) Assessment of factors influencing surface roughness on the machining of Al/SiC particulate composites. Mater Des 28:1584–1591
10. Gallab ME, Skallad M (1998) Machining of Al/SiC particulate metal matrix composites part II: work piece integrity. J Mater Process Technol 83:277–285
11. Ge YF, Xu JH, Yang H (2010) Diamond tools wear and their applicability when ultra-precision turning of SiCp/2009Al matrix composite. Wear 269:699–708
12. Yang YF, Wu Q, Zhan ZB, Li L, He N, Shrestha R (2015) An experimental study on milling of high-volume fraction SiCP/Al composites with PCD tools of different grain size. Int J Adv Manuf Technol 79:1699–1705
13. Davim JP (2002) Diamond tool performance in machining metal–matrix composites. J Mater Process Technol 128:100–105
14. Davim JP, Silva J, Baptista AM (2007) Experimental cutting model of metal matrix composites (MMCs). J Mater Process Technol 183: 358–362
15. Dandekar CR, Shin YC (2013) Multi-scale modeling to predict subsurface damage applied to laser-assisted machining of a particulate reinforced metal matrix composite. J Mater Process Technol 213: 153–160
16. Zhu Y, Kishawy HA (2005) Influence of alumina particles on the mechanics of machining metal matrix composite during machining. Int J Mach Tools Manuf 45:389–398
17. Pramanik A, Zhang LC, Arsecularatne JA (2007) An FEM investigation into the behavior of metal matrix composites: tool-particle interaction during orthogonal cutting. Int J Mach Tools Manuf 47: 1497–1506
18. Xiong YF, Wang WH, Jiang RS, Lin KY, Song GD (2016) Surface integrity of milling in-situ TiB2 particle reinforced Al matrix composites. Int J Refract Met Hard Mater 54:407–416
19. Fan XL, Suo T, Sun Q, Wang TJ (2013) Dynamic mechanical behavior of 6061 Al alloy at elevated temperatures and different strain rates. Acta Mech Solida Sin 26:111–120
20. Tan YQ, Yang DM, Sheng Y (2009) Discrete element method (DEM) modeling of fracture and damage in the machining process of polycrystalline SiC. J Eur Ceram Soc 29:1029–1037
21. Ghandehariun A, Kishawy HA, Umer U, Hussein HM (2016) On tool–workpiece interactions during machining metal matrix composites: investigation of the effect of cutting speed. Int J Adv Manuf Technol 84:2423–2435
22. Wang T, Xie LJ, Wang XB, Shang TY (2015) 2D and 3D milled surface roughness of high volume fraction SiCp/Al composites. Defence Technol 11:104–109
23. Zhou L, Hou N, Huang ST, Xu LF (2014) An experimental study on formation mechanisms of edge defects in orthogonal cutting of SiCp/Al composites. Int J Adv Manuf Technol 72:1407–1414
24. Zhang XX, Ni DR, Xiao BL, Andra H, Gan WM, Hofmannd M, Ma ZY (2015) Determination of macroscopic and microscopic residual stresses in friction stir welded metal matrix composites via neutron diffraction. Acta Mater 87:161–173
25. Dabade UA, Joshi SS, Balasubramaniam R, Bhanuprasad VV (2007) Surface finish and integrity of machined surfaces on Al/SiCp composites. J Mater Process Technol 192-193:166–174
26. Pramanik A, Zhang LC, Arsecularatne JA (2008) Machining of metal matrix composites: effect of ceramic particles on residual stress, surface roughness and chip formation. Int J Mach Tools Manuf 48:1613–1625
27. Salahshoor M, Guo YB (2014) Finite element simulation and experimental validation of residual stresses in high speed dry milling of biodegradable magnesium-calcium alloys. Int J Mech Sci 80: 153–159
28. Arrazola PJ, Kortabarria A, Madariaga A, Esnaola JA, Fernandez E, Cappellini C, Ulutan D, Özel T (2014) On the machining induced residual stresses in IN718 nickel-based alloy: experiments and predictions with finite element simulation. Simul Model Pract Th 41:87–103
29. Capello E (2005) Residual stress in turning, part I: influence of process parameters. J Mater Process Technol 160:221–228